IIETA International Information and Engineering Technology Association
Advancing the World of Information and Engineering

Journal of New Materials for Electrochemical Systems
Vol. 26, No.2, April 2023, pp.139-144
Journal homepage: http://iieta.org/journals/jnmes

$SrTiO_3$ Perovskite-Based Coating on AZ31 Alloy and Its Characterization

Y L Raja Mohan[1], S. Parameswari[2], P. Karpagavinayagam[3], S. Thanikaikarasan[4] , C. Vedhi[3*], A. Cyril[5*]

[1]Department of Industrial Chemistry, Alagappa University, Karaikudi-3, Tamil Nadu, India
2 Department of Chemistry, Indira Institute of Engineering and Technology, Chennai, Tamil Nadu, India
[3] PG & Research Department of Chemistry, V. O Chidambaram College, Thoothukudi-8, Tamil Nadu, India
[4]Department of Physical Sciences, Saveetha School of Engineering, SIMATS, Chennai – 602 105, Tamil Nadu, India.
[5]PG & Research Department of Chemistry, Raja Dorasingam Government Arts College, Sivaganga, Tamil Nadu, India
Corresponding Author Email: cyrilchemistry@gmail.com: cvedhi23@gmail.com

https://doi.org/10.14447/jnmes.v26i2.a09

Received: July 11, 2022
Accepted: January 10, 2023

Keywords:
AZ31; $SrTiO_3$; Silicone resign; Corrosion; Impedance

ABSTRACT

Herein, the nanoparticles of $SrTiO_3$perovskite oxide were synthesized using simple hydrothermal process. The synthesized perovskite oxide material was characterized by XRD and FTIR techniques. The XRD analysis reveals that the formed $SrTiO_3$ perovskite oxide in cubic crystal phase with high phase purity. The FTIR result demonstrate the stretching and vibration bands of Ti-O and Sr-O along with O-H functional groups. The $SrTiO_3$perovskite oxide powder was added to silicone resin and the paste was applied on AZ31 alloy sample, which was then used for electrochemical analysis. The corrosion characteristics of $SrTiO_3$perovskite oxide coating over AZ31 alloy were investigated in 7 % NaCl electrolyte, wherein platinum foil used as counter electrode, saturated calomel electrode (SCE) as reference and $SrTiO_3$perovskite oxide coated AZ31 alloy as working electrode. The results reveal that the open circuit potential of AZ31 alloy shifted from -1.57 V (SCE) to -0.95 V (SCE). The corrosion rates of bare AZ31 alloy calculated and found as 7 x 10^{-2} mA/cm^2, while the same after coating was measured as 9 x 10^{-6} mA/cm^2. The electrochemical impedance results also reveal that corrosion protection induced by the coating. Hence, it is summarized that the $SrTiO_3$perovskite oxide coating demonstrated improved corrosion resistance for AZ31 alloy.

1. INTRODUCTION

Magnesium alloys have light weight and high density, which makes them applicable in various applications such as aerospace and automobile sectors. Nevertheless, having the said advantages, the magnesium and it's alloys suffer higher corrosion in many mediums due to the more electromotive force in series [1-4]. Hence, research and development efforts are directed to improve the corrosion resistance of Mg in various methods such as addition of allying elements and protective coatings [5-12]. The development of protective coatings on magnesium alloys found as easy and economically favorable process [13-15]. Ren et al developed calcium deficient hydroxyapatite (CDHA) layer on AZ31 alloy, which the mass loss of AZ31 alloy is reduced in SBF solution [13]. Hanas et al developed polycaprolactone (PCL) nano-fibrous layer coatings using electrospinning technique. The results shows that nano-fibres PCL coating showed improved corrosion resistance [14]. Zhang et al developed Mg–Al-layered double hydroxide (LDH) coatings using both co-precipitation and hydrothermal process, wherein the LDH coatings showed nano flake structure arranged vertically, which shoed excellent corrosion resistance performance [15]. Huang et al studied the photo-effect on the corrosion properties of $SrTiO_3$ coatings using hot dipped process on zinc coated steel. The results shows that the $SrTiO_3$ coatings demonstrated reducing photo-corrosion effect of zinc coated steel [16]. The Effect of $SrTiO_3$ coatings on AZ31 alloy has not explored till the date.

2. MATERIALS AND METHODS

2.1. Chemicals

Strontium hydroxide $Sr(OH)_2{\cdot}8H_2O$ was purchased Sigma Aldrich, Titanium chloride ($Ti(OH)_4$)was purchased from Merck and Silicone resin 1805was purchased from Dow Corning.

2.2. Sample preparation

The AZ31 alloy was cut into the dimensions of 12 x 12 x 3 mm from the sheet and polished using SiC grit papersand finally with 1 and 0.5 diamond paste. In the process, the samples were exposed to 200 SiC grit paper and extended the process further up to 1200 grit paper polishing, in the end, 1- and 0.5-microns diamond paste polishing was carried out. The samples were washed with water to remove the polish impurities.

2.3. Electrode preparation

The synthesized $SrTiO_3$ nano powder (1g) was mixed with silicone resin (10 ml) and mixed well to prepare paste (semi viscous). The paste was applied to the polished AZ31 alloy by doctor blade method and dried. The coated samples were then mounted with copper wire for electrochemical studies.

2.4.Electrochemical experiments

The electrochemical studies involving open circuit potential, polarization and impedance analysis were carried out on bare AZ31 alloy and $SrTiO_3$ perovskite oxide coated AZ31 alloy. For this, a three-electrode system was used in which platinum foil as counter electrode, saturated calomel as reference electrode and AZ31 alloy (with and without coating) used as working electrode in 7% NaCl medium.

3.RESULTS AND DISCUSSION

3.1. X-ray diffraction analysis

In order to understand the crystallography of bare AZ31 and $SrTiO_3$ perovskite oxide coated AZ 31 alloy, X-ray diffraction technique was employed over samples and the patterns were recorded with Cu Kαof 1.5418 Å.
The XRD pattern of bare AZ31 alloy is shown in Figure 1. The figure shows the sharp peaks indicating high crystalline nature of Mg alloy. It is also noticed that the preferential growth in (101) plane. The peaks are well matched with standard fileJCPDS file no 35-0821, which shows the hexagonal crystal structure a=b=3.2094 Å and c=5.211Å and belongs to P63/mmc space group [17-20].

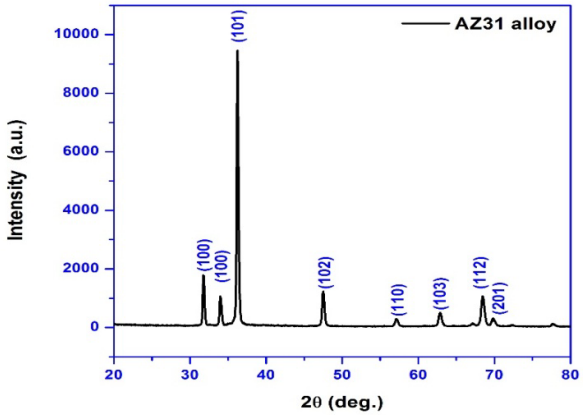

Figure 1: XRD pattern of bare AZ31 alloy

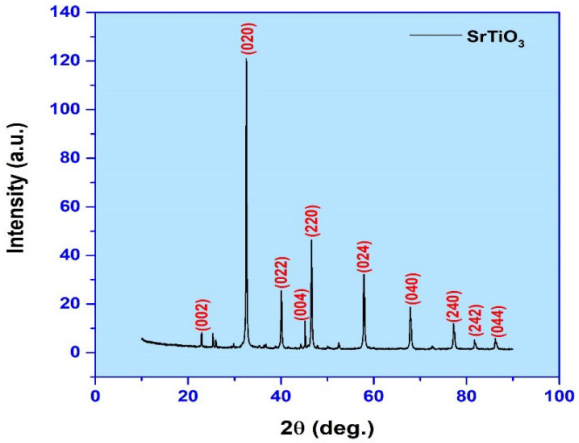

Figure 2: XRD pattern of $SrTiO_3$ perovskite oxide coated AZ 31 alloy

Figure 2 demonstrate the high crystallinity for $SrTiO_3$ perovskite material. The peals are well matched with standard file JCPDF # 05-0634, which shows the cubic perovskite crystal structure (a = b = c = 3.90 Å) belongs to Pm3m (221) space group [21-24].

3.2. Surface morphology

The surface morphology of $SrTiO_3$ perovskite oxide is shown in Figures 3-5. It is noticed that the nano particles are well distributed. The shape of the particles are irregular and the size is varied among them.

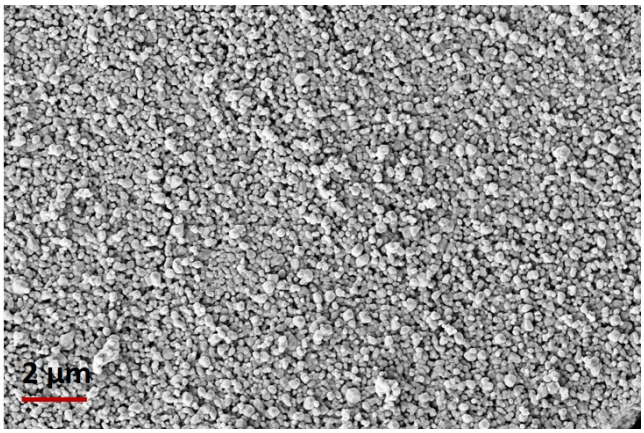

Figure 3: Surface morphology of $SrTiO_3$ perovskite oxide

The higher magnified images showing the surface morphology of $SrTiO_3$ perovskite oxide shows the distinct features, which includes nano sized particles. The crystal growth shows there is no much effect of surfactant in the synthesis of $SrTiO_3$ perovskite oxide.

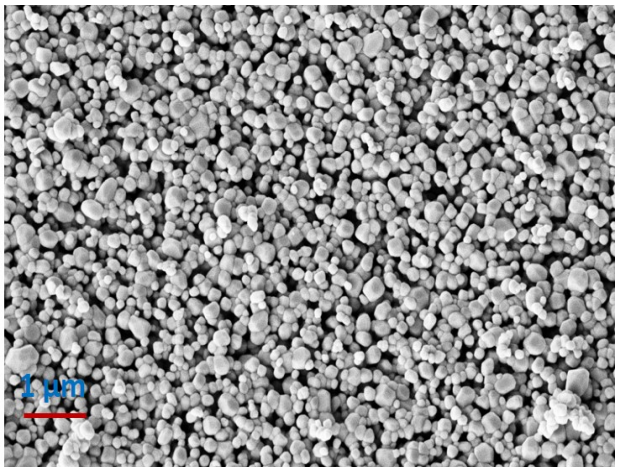

Figure 4: Surface morphology of $SrTiO_3$ perovskite oxide at higher magnification

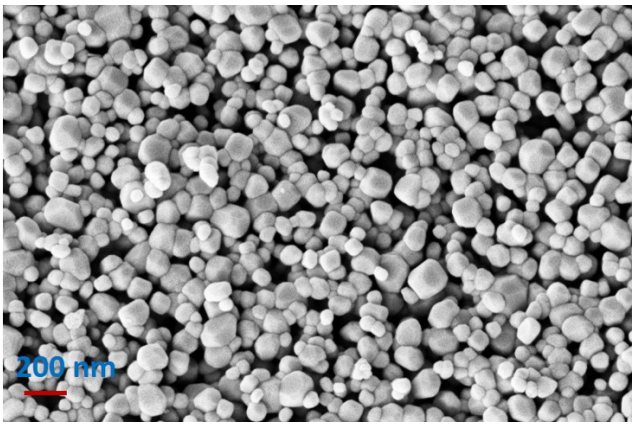

Figure 5: Surface morphology of $SrTiO_3$ perovskite oxide at higher magnification

As mentioned in the XRD analysis, the powders are free from impurities and the figures show the shape and size of particles, which corresponds to purely $SrTiO_3$ perovskite oxide. In many applications, the nano sized particles provide better performance, however, in the current study, the nano sized particles provided high dense packing in the coatings.

3.3. HRTEM analysis

The morphological images acquired through high resolution transmission electron microscope images is shown in Figure 6

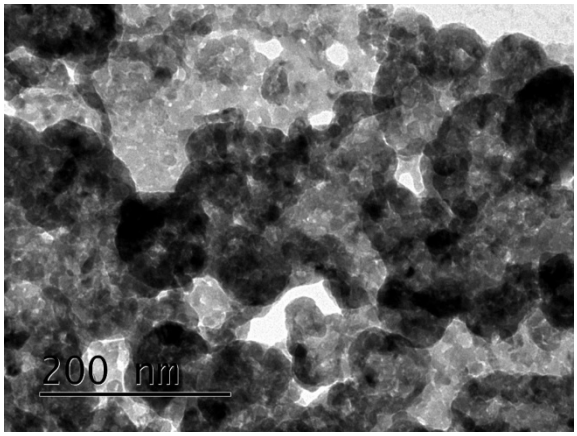

Figure 6: HRTEM images of $SrTiO_3$ perovskite oxide

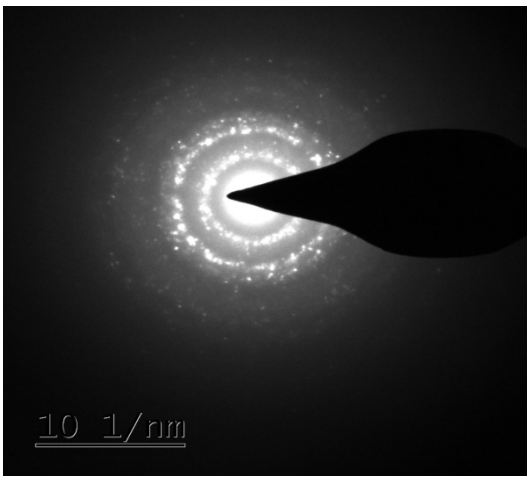

Figure 7: SAED pattern of $SrTiO_3$perovskite oxide

Figure 6 reveals that the nanoparticles are clubbed together and showed as micro-sized particle. However, the individual particles are clearly demonstrating the nanosize nature in high resolution transmission electron microscopic analysis. The $SrTiO_3$ perovskite oxide powder was sonicated and deposited on the Cu grid and examined the morphological features in HRTEM. The figure 7 reveals the polycrystalline nature of SrTiO3 perovskite oxide.

3.4. FTIR analysis

The FTIR spectrum of $SrTiO_3$perovskite oxideis shown in Figure 8. The peaks are noticed at 450, 580, 760, 1456 and 3440 cm^{-1}.

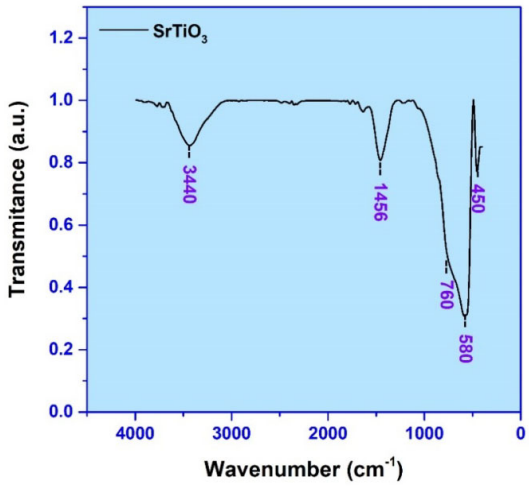

Figure 8: FTIR spectrum of $SrTiO_3$perovskite oxide

The peak at 450 cm^{-1} is obtained due to the stretching mode of Ti-O. The bands at 1450 is correspond to the vibration C-O in $-CO_3^{2-}$ due to presence trace $SrCO_3$[22-27]. The band at 3440 cm^{-1}represents the O-H group which is resulted from physically adsorbed water.

3.5. Electrochemical analysis

The open circuit potentials of AZ31 and $SrTiO_3$ perovskite oxide coated AZ31 alloy are studied with respect to time and presented in Figure 9 and 10, respectively. It is noticed that the open circuit potential of AZ31 alloy is -1.64 V (SCE) and the same $SrTiO_3$ perovskite oxide coated AZ31 alloy is -0.95 V (SCE). The noble side shift in potential is clearly noticed, which indicate the enhancement in corrosion protection.

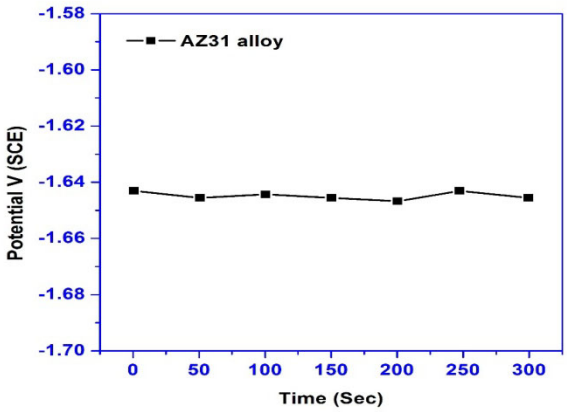

Figure 9: Open circuit potentials of bare AZ31 alloy

The OCP was highly unstable due to the evolution of hydrogen gas on the surface reaction of pure Mg alloy. However, the presented values are smoothened and represented in Figure 9.

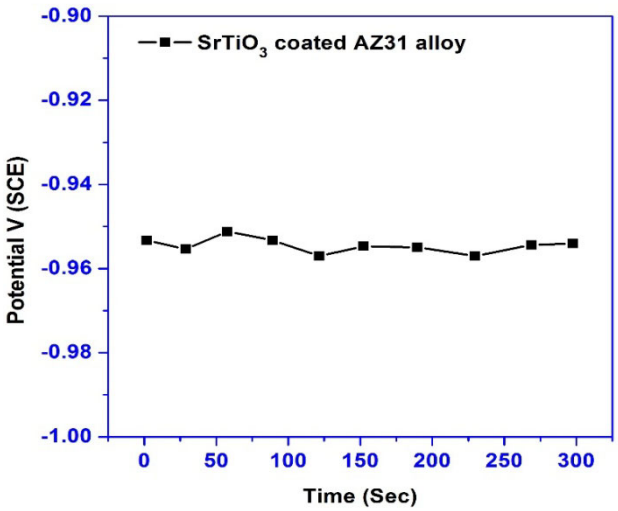

Figure 10: Open circuit potentials of $SrTiO_3$ perovskite oxide coated AZ31 alloy

The $SrTiO_3$ perovskite oxide coated AZ31 alloy shows the corrosion potential around -0.95 V (SCE).This feature clearly indicate that the perovskite coating is beneficial as the corrosion potential shifted to more noble direction, which shows the higher corrosion protection induced due to the coating.

The corrosion rates of bare AZ31 alloy and $SrTiO_3$coated AZ31 alloy were studied and the corrosion behavior is shown in Figure 11.

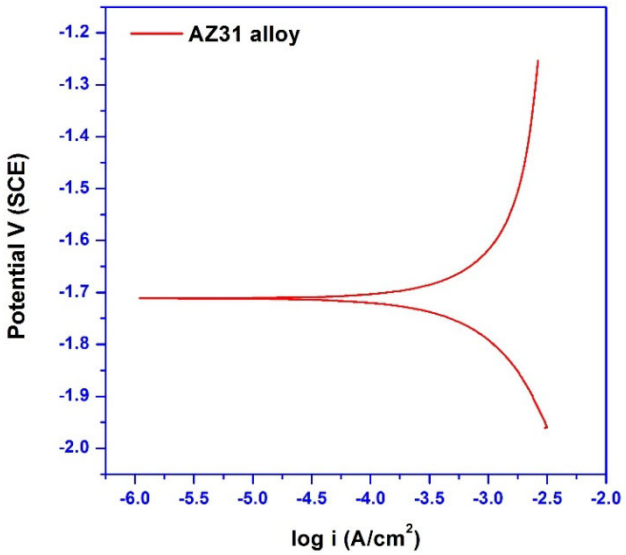

Figure 11: Tafel plot of bare AZ31 alloy

From the Figure 11, it is noticed that corrosion potential is noticed that bare AZ31 demonstrated the corrosion rate 3.4 x 10^{-4} mA/cm^2. The corrosion rates were calculated using the software and interpretated. Both the anodic and cathodic curves indicate that Mg alloy involved in chemical reaction with the electrolyte and produced hydrogen cathodically and some notable passivation observed in anodic region.

Further, the corrosion rate of $SrTiO_3$ perovskite oxide coated AZ31 alloy measured from the Tafel plot which is shown in Figure 12. The calculated corrosion rate of coatings is found as 9 x 10^{-6} mA/cm^2.

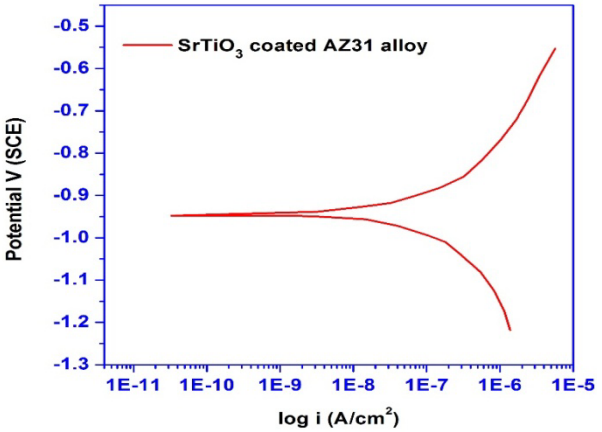

Figure 12: Tafel plot of $SrTiO_3$ perovskite oxide coated AZ31 alloy.

From the Figure, it is noticed that corrosion potential is noticed that $SrTiO_3$ perovskite oxide coated AZ31 demonstrated the corrosion rate 9 x 10^{-6} mA/cm^2. There is significant reduction in the corrosion rate after applying the $SrTiO_3$ perovskite oxide coating. The shift of Ecorr into noble direction implies that enhanced corrosion protection. The perovskite coating shoed less corrosion rates in the NaCl medium.

In addition to this, the electrochemical impedance curves of bare AZ31 and $SrTiO_3$perovskite oxide coated AZ31 alloyare shown Figures13 and 14, respectively. The Nyquist results show that the corrosion resistance is increased for the $SrTiO_3$ perovskite oxide coated AZ31 alloy in comparison with bare AZ31 alloy.

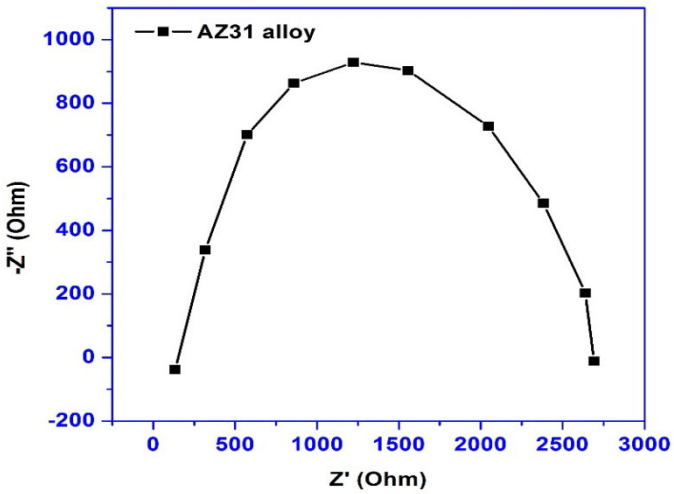

Figure 13: Electrochemical impedance curves of bare AZ31 alloy

The impedance curve as Nyquist plot is noticed in the images 13. The Nyquist curve shows the full half circle. The curve was fit with randles equivalent circuit model as shown below.

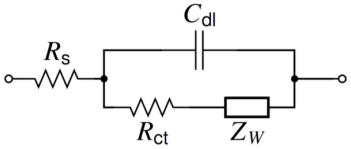

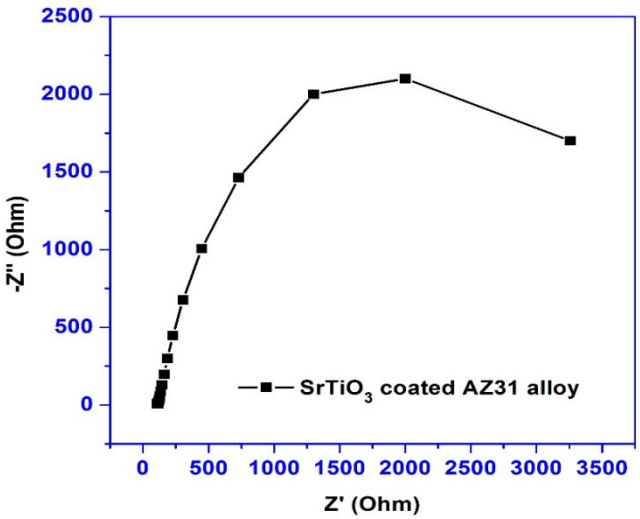

Figure 14: EIS-Nyquist plots of bare AZ31 and $SrTiO_3$perovskite oxide coated AZ31 alloy

The Nyquist plot of $SrTiO_3$ perovskite oxide coated AZ31 alloy showed half circle and best fit to randles equivalent circuit model. The resistance measurements indicate that the bare AZ31 alloy showed very less corrosion resistance, while the$SrTiO_3$ perovskite oxide coated AZ31 alloy showed superior corrosion resistance.

4. CONCLUSIONS

The nanoparticles of$SrTiO_3$perovskite oxide was synthesized using hydrothermal route.

The $SrTiO_3$perovskite oxide-basedcoatings were developed on AZ31 alloy using silicone resin.

The bare AZ31 alloy showed corrosion current densityas 3.4 x 10^{-4}mA/cm^2, while the same for $SrTiO_3$perovskite oxide coated AZ31 alloy noticed as9 x10^{-6} A/cm^2.

The results reveal that the $SrTiO_3$perovskite oxide coated AZ31 alloy demonstrated higher corrosion resistance than that of bare AZ31 alloy.

REFERENCE

[1] Mordike, B, & Ebert, T. (2001). Magnesium. Materials Science and Engineering: A, 302(1), 37–45. doi:10.1016/s0921-5093(00)01351-4.

[2] Thomas, S., Medhekar, N. V., Frankel, G. S., &Birbilis, N. (2015). Corrosion mechanism and hydrogen evolution on Mg. Current Opinion in Solid State and Materials Science, 19(2), 85–94. doi:10.1016/j.cossms.2014.09.005.

[3] Wu, R., Yan, Y., Wang, G., Murr, L. E., Han, W., Zhang, Z., & Zhang, M. (2014). Recent progress in magnesium–lithium alloys. International Materials Reviews, 60(2), 65–100. doi:10.1179/1743280414y.0000000044.

[4] Tokunaga, T., Ohno, M., & Matsuura, K. (2018). Coatings on Mg alloys and their mechanical properties: A review. Journal of Materials Science & Technology, 34(7), 1119–1126. doi:10.1016/j.jmst.2017.12.004.

[5] Singh Raman, R. K., Birbilis, N., &Efthimiadis, J. (2004). Corrosion of Mg alloy AZ91 – the role of microstructure. Corrosion Engineering, Science and Technology, 39(4), 346–350. doi:10.1179/174327804x13208.

[6] Esmaily, M., Shahabi-Navid, M., Svensson, J.-E., Halvarsson, M., Nyborg, L., Cao, Y., & Johansson, L.-G. (2015). Influence of temperature on the atmospheric corrosion of the Mg–Al alloy AM50. Corrosion Science, 90, 420–433. doi:10.1016/j.corsci.2014.10.040.

[7] Esmaily, M., Blücher, D. B., Lindström, R. W., Svensson, J.-E., & Johansson, L. G. (2015). The Influence of SO2on the Corrosion of Mg and Mg-Al Alloys. Journal of The Electrochemical Society, 162(6), C260–C269. doi:10.1149/2.0801506jes.

[8] Pu, Z., Yang, S., Song, G.-L., Dillon, O. W., Puleo, D. A., &Jawahir, I. S. (2011). Ultrafine-grained surface layer on Mg–Al–Zn alloy produced by cryogenic burnishing for enhanced corrosion resistance. Scripta Materialia, 65(6), 520–523. doi:10.1016/j.scriptamat.2011.06.013.

[9] Danaie, M., Asmussen, R. M., Jakupi, P., Shoesmith, D. W., &Botton, G. A. (2014). The cathodic behaviour of Al–Mn precipitates during atmospheric and saline aqueous corrosion of a sand-cast AM50 alloy. Corrosion Science, 83, 299–309. doi:10.1016/j.corsci.2014.02.030.

[10] Asmussen, R. M., Jakupi, P., Danaie, M., Botton, G. A., &Shoesmith, D. W. (2013). Tracking the corrosion of magnesium sand cast AM50 alloy in chloride environments. Corrosion Science, 75, 114–122. doi:10.1016/j.corsci.2013.05.022.

[11] Esmaily, M., Mortazavi, N., Shahabi-Navid, M., Svensson, J. E., Johansson, L. G., &Halvarsson, M. (2015). On the capability of in-situ exposure in an environmental scanning electron microscope for investigating the atmospheric corrosion of magnesium. Ultramicroscopy, 153, 45–54. doi:10.1016/j.ultramic.2015.02.010.

[12] Kim, J. I., Nguyen, H. N., You, B. S., & Kim, Y. M. (2019). Effect of Y addition on removal of Fe impurity from magnesium alloys. Scripta Materialia, 162, 355–360. doi:10.1016/j.scriptamat.2018.11.046.

[13] Yaowei, Y., Wei, F., Xiang, Z., Qilin, D., &Jianguo, Y. (2017). In-situ Synthesis of WC/TaC Reinforced Nickel-Based Composite Alloy Coating by Laser Cladding. Rare Metal Materials and Engineering, 46(11), 3176–3181. doi:10.1016/s1875-5372(18)30024-9.

[14] Wu, G., Dai, W., Zheng, H., & Wang, A. (2010). Improving wear resistance and corrosion resistance of AZ31 magnesium alloy by DLC/AlN/Al coating. Surface and Coatings Technology, 205(7), 2067–2073. doi:10.1016/j.surfcoat.2010.08.103.

[15] Han, B. (2017). A Composite Anodic Coating Containing Graphene on AZ31 Magnesium Alloy. International Journal of Electrochemical Science, 9829–9843. doi:10.20964/2017.10.30.

[16] Avedesian, M.M. Baker, H. ASM Specialty Handbook, Magnesium and Magnesium Alloys, ASM International, USA, 1999.

[17] Sivashanmugam, N., &Harikrishna, K. L. (2020). Influence of Rare Earth Elements in Magnesium Alloy - A Mini Review. Materials Science Forum, 979, 162–166. doi:10.4028/www.scientific.net/ MSF.979.162.

[18] Friedrich H.E., Mordike B.L. Magnesium Technology: Metallurgy, Design, Data, Applications, Magnesium Technology, Springer, Germany, 2006. Springer-Verlag Berlin Heidelberg, 2006. 647 p

[19] Sunil, B. R., Ganesh, K. V., Pavan, P., Vadapalli, G., Swarnalatha, C., Swapna, P., Pradeep Kumar Reddy, G. (2016). Effect of aluminum content on machining characteristics of AZ31 and AZ91 magnesium alloys during drilling. Journal of Magnesium and Alloys, 4(1), 15–21. doi:10.1016/j.jma.2015.10.003.

[20] B.R. Sunil, K.V. Ganesh, P. Pavan, G. Vadapalli, C. Swarnalatha, P. Swapna, P.Bindukumar, G. Pradeep Kumar Reddy, (2016). Journal of Magnesium and Alloys, 4(1), 15–21.

[21] C. J. Dalmaschio, C. Ribeiro, and E. R. Leite, "Impact of the colloidal state on the oriented attachment growth mechanism," Nanoscale, vol. 2, no. 11, pp. 2336–2345, 2010

[22] M. Niederberger and H. Colfen, "Oriented attachment and mesocrystals: non-classical crystallization mechanisms based on nanoparticle assembly," Physical Chemistry Chemical Physics, vol. 8, no. 28, pp. 3271–3287, 2006

[23] Wei, H., Cai, J., Zhang, Y., Zhang, X., Baranova, E. A., Cui, J.,Wu, Y. (2020). Synthesis of $SrTiO_3$ submicron cubes with simultaneous and competitive photocatalytic activity for H_2O splitting and CO_2 reduction. RSC Advances, 10(70), 42619–42627. doi:10.1039/d0ra08246e.

[24] Fujinami, K., Katagiri, K., Kamiya, J., Hamanaka, T., &Koumoto, K. (2010). Sub-10 nm strontium titanate nanocubes highly dispersed in non-polar organic solvents. Nanoscale, 2(10), 2080. doi:10.1039/c0nr00543f.

[25] Macounová, K. M., Nebel, R., Klusáčková, M., Klementová, M., &Krtil, P. (2019). Selectivity Control of the Photo-Catalytic Water Oxidation on SrTiO3 Nanocubes via Surface Dimensionality. ACS Applied Materials & Interfaces, 11(18), 16506–16516. doi:10.1021/acsami.9b00342.

[26] Zhou, M., Chen, J., Zhang, Y., Jiang, M., Xu, S., Liang, Q., & Li, Z. (2019). Shape-controlled synthesis of golf-like, star-like, urchin-like and flower-like SrTiO3 for highly efficient photocatalytic degradation and H2 production. Journal of Alloys and Compounds, 152796. doi:10.1016/j.jallcom.2019.152796

[27] Piskunov, S., Heifets, E., Eglitis, R. ., &Borstel, G. (2004). Bulk properties and electronic structure of SrTiO3, BaTiO3, PbTiO3 perovskites: an ab initio HF/DFT study. Computational Materials Science, 29(2), 165–178. doi:10.1016/j.commatsci.2003.08.036.